THE JOURNAL OF BIOLOGICAL CHEMISTRY VOL. 284, NO. 36, pp. 24634–24643, September 4, 2009

Structural Investigation of the Interaction between LolA and LolB Using NMR[S]

Received for publication, April 1, 2009, and in revised form, June 15, 2009 Published, JBC Papers in Press, June 22, 2009, DOI 10.1074/jbc.M109.001149

Shingo Nakada[‡§], Masayoshi Sakakura[§], Hideo Takahashi[¶], Suguru Okuda[‖], Hajime Tokuda[‖], and Ichio Shimada[§¶1]

From the [‡]Laboratory of Genomic Science, Dainippon Sumitomo Pharma, Ltd., 33-94, Enoki, Suita, Osaka 564-0053, [§]Graduate School of Pharmaceutical Sciences, The University of Tokyo, 7-3-1, Hongo, Bunkyo-ku, Tokyo 113-0033, [¶]Biomedicinal Information Research Center, National Institute of Advanced Industrial Science and Technology, Aomi, Koto-ku, Tokyo 135-0064, and [‖]Institute of Molecular and Cellular Biosciences, The University of Tokyo, Yayoi, Bunkyo-ku, Tokyo 113-0032, Japan

Lipoproteins that play critical roles in various cellular functions of Gram-negative bacteria are localized in the cells inner and outer membranes. Lol proteins (LolA, LolB, LolC, LolD, and LolE) are involved in the transportation of outer membrane-directed lipoproteins from the inner to the outer membrane. LolA is a periplasmic chaperone that transports lipoproteins, and LolB is an outer membrane receptor that accepts lipoproteins. To clarify the structural basis for the lipoprotein transfer from LolA to LolB, we examined the interaction between LolA and mLolB, a soluble mutant of LolB, using solution NMR spectroscopy. We determined the interaction mode between LolA and mLolB with conformational changes of LolA. Based upon the observations, we propose that the LolA·LolB complex forms a tunnel-like structure, where the hydrophobic insides of LolA and LolB are connected, which enables lipoproteins to transfer from LolA to LolB.

Gram-negative bacteria express lipid-modified proteins, lipoproteins, which are anchored to the cellular membrane via acyl chains attached to N-terminal cysteine residues of the lipoproteins. Putative lipoproteins have been found in various bacteria. For example, *Escherichia coli* has at least 90 types of lipoproteins (1), and the Lyme disease spirochete *Borrelia burgdorferi* has 105 putative lipoproteins (2). Although little is known about the functions of the majority of lipoproteins, some of the lipoproteins play essential roles in various cellular functions of Gram-negative bacteria, such as cell surface structure stabilization, cell shape maintenance, substrate transport, cell growth, and cell signaling (3).

Lipoproteins are located at three cellular membrane sites; they are the periplasmic side of the inner membrane, the periplasmic side of the outer membrane, and the outside of the outer membrane (4). In *E. coli* most of the lipoproteins are anchored to the periplasmic side of the outer membrane, whereas others are anchored to that of the inner membrane (1). Therefore, the transportation of the lipoproteins to the outer membrane is essential for *E. coli*.

Five Lol proteins, LolA, LolB, LolC, LolD, and LolE, play central roles in the outer membrane-directed lipoprotein localization. The Lol·CDE complex, which is anchored to the inner membrane, transfers the lipoproteins from the membrane to a soluble monomer periplasmic protein, LolA (182 amino acids) in an ATP-dependent manner (5–7). LolA transports the lipoproteins from the inner membrane through the periplasmic space to the outer membrane and transfers them to an outer membrane lipoprotein, LolB (186 amino acids). LolB is anchored to the membrane by acyl chains attached to its N-terminal cysteine, and it finally inserts the lipoproteins into the outer membrane (8–10).

Among the Lol proteins the crystal structures of LolA and LolB have been solved. As for LolB, the soluble mutant of LolB, mLolB, in which the N-terminal cysteine residue was replaced with an alanine residue, was used for the structural analysis. Although LolA and mLolB share only 8% primary sequence identity, their tertiary structures are similar to each other (11). The structures of both LolA and mLolB resemble an open β-barrel with a lid. The convex side of the β-barrel is fully solvent-exposed, whereas the concave side is partly exposed (supplemental Fig. S1).

The open β-barrels of LolA and LolB comprise 11 antiparallel β-strands ($\beta1$–$\beta11$) and an extra β-strand, $\beta12$ for LolA and $\beta11'$ for LolB. The lid is composed of three α-helices ($\alpha1$–$\alpha3$) and is embedded in the concave side of the β-barrel. The concave sides of LolA and LolB contain many hydrophobic residues. Therefore, this concave side of the proteins is speculated to be the binding site for the hydrophobic acyl chains of lipoproteins. Interestingly, one of the crystal structures of LolB accommodated a molecule of polyethylene glycol 2000 monomethyl ether, PEGMME2000, on the hydrophobic surface of the concave side (supplemental Fig. S1).

The specific interaction between LolA and LolB is a decisive step in correctly sorting lipoproteins from LolA via LolB to the outer membrane. However, the structural aspects of the interaction, which would clarify how LolA transfers lipoproteins to LolB, remain unknown. To address this issue, we focused on the interaction between LolA and LolB.

Here we investigated the interaction of LolA with LolB by NMR spectroscopy. We used LolA with a His_6 tag and mLolB, which retain the biological activities similar to those of the wild type protein (8, 12). By exploiting the cross-saturation and

[S] The on-line version of this article (available at http://www.jbc.org) contains supplemental Tables S1–S4 and Figs. S1–S4.

[1] To whom correspondence should be addressed: Graduate School of Pharmaceutical Sciences, The University of Tokyo, 7-3-1, Hongo, Bunkyo-ku, Tokyo 113-0033, Japan. Tel.: 81-3-5841-4810; Fax: 81-3-5841-4811; E-mail: shimada@iw-nmr.f.u-tokyo.ac.jp.

paramagnetic relaxation enhancement (PRE)[2] techniques, we successfully determined the interfacial residues of LolA and mLolB and the relative orientation of the two molecules in the complex. In addition, we identified the binding sites of an acyl chain analogue, decanoate, on LolA and mLolB. The results obtained from the present study not only explain how LolA might achieve lipoprotein transfer to LolB but also may provide new insights into the structural and functional aspects of other fatty acid-binding proteins.

EXPERIMENTAL PROCEDURES

LolA and mLolB Sample Preparation—E. coli BL21 (DE3) Gold (Stratagene) cells were transfected with the plasmid bearing the LolA or mLolB gene (13, 14). For unlabeled LolA or mLolB, the cells were grown in Luria-Bertani broth. For proteins uniformly labeled with ^{2}H and ^{15}N and/or ^{13}C, the cells were grown in M9 minimal medium containing $^{15}NH_4Cl$ (1 g liter^{-1}; Spectra Stable Isotopes) and [$^{2}H_6$]glucose or [$^{13}C_6$/$^{2}H_6$]glucose (98% labeled; 3 g liter^{-1}; Spectra Stable Isotopes) in 99% D_2O. LolA and mLolB were purified as described elsewhere (13, 14).

Inhibition of Lipoprotein Transfer from LolA to mLolB by Decanoate—The inhibitory effect of decanoate (Sigma) on the incorporation of lipoproteins into the outer membrane was examined. A spheroplast supernatant containing the LolA·[^{35}S]L10P complex was mixed with 0.2 mg ml^{-1} LolB-depleted outer membranes, as described previously (5, 15–18). mLolB (0.08 μg) was pretreated with the specified concentrations of decanoate in 20 mM Tris-HCl (pH 7.5) for 3 h on ice. A 10-μl aliquot of this decanoate-treated mLolB solution was added to 90 μl of a mixture containing the LolA·[^{35}S]L10P complex and outer membranes followed by incubation at 30 °C for 1 h. The membrane incorporation of [^{35}S]L10P was examined by SDS-PAGE and fluorography as described (15) after fractionation into pellet and supernatant by centrifugation at 100,000 × *g* for 30 min.

Chemical Shift Perturbation Experiments of LolA and mLolB upon Decanoate Addition—We conducted chemical shift perturbation experiments of LolA and mLolB upon the addition of decanoate. Decanoate was titrated to ^{15}N-labeled samples of LolA (0.28 mM) or mLolB (0.28 mM), and each ^{1}H,^{15}N TROSY spectrum was recorded. The weighted sum of the ^{1}H and ^{15}N chemical shift changes for each residue was calculated with the equation $\Delta\delta_{wei} = \Delta\delta(^{1}HN) + 0.2\,\Delta\delta(^{15}N)$ upon the addition of 5 mM decanoate.

Isothermal Titration Calorimetry Experiment—To determine the dissociation constant (K_d) of the LolA·mLolB complex, we conducted isothermal titration calorimetry measurements using a VP-ITC (MicroCal) instrument at 25 °C. LolA and mLolB samples were prepared in a buffer containing 66 mM sodium phosphate (pH 6.9) and 100 mM NaCl. mLolB was injected into LolA in 29 aliquots of 10 μl each at 240-s intervals. The data acquired from the mLolB injections into the buffer were subtracted from the experimental data. The data were analyzed using the MicroCal Origin software.

NMR Samples, Assignments, and Chemical Shift Perturbation Experiments of LolA and mLolB—NMR samples (0.3–0.5 ml) were prepared using 0.3–2.0 mM LolA and/or mLolB in the following buffers. For the assignments of LolA in the LolA·mLolB complex and the chemical shift perturbation experiments of LolA with mLolB or decanoate, NMR samples (0.3–0.5 ml) using buffer A (66 mM sodium phosphate (pH 6.9), 100 mM NaCl) were used. For other NMR measurements buffer B (38 mM 2-morpholinoethanesulfonic acid (pH 6.9) was used. For cross-saturation experiments buffer B contained 60% $^{2}H_2O$. For other NMR experiments the buffers contained 10% $^{2}H_2O$.

For the dimensional NMR experiments of the LolA assignments in the complex state with mLolB, a Bruker AVANCE 800 MHz spectrometer was used. For the cross-saturation experiments, a Bruker AVANCE 600 MHz spectrometer with a cryogenic probe was used. For the other NMR experiments, a Varian UNITY-INOVA 500 MHz spectrometer was used. All NMR spectra were recorded at 37 °C. Backbone resonance assignments of LolA and mLolB in the free state were performed as described elsewhere (13, 14). The assignments of LolA and mLolB in the LolA·mLolB complex were derived from titration experiments, and the assignments of free state LolA and mLolB were supported by three-dimensional NMR experiments.

In the titration experiments ^{1}H,^{15}N TROSY spectra of the labeled LolA or mLolB with a series of concentrations of the unlabeled binding partner were measured. The molar ratios of unlabeled mLolB or LolA to labeled LolA or mLolB were varied from 0 to 5.5. At the molar ratio of 3:1 (unlabeled protein/labeled protein), where no more chemical shift changes of the labeled proteins occurred, the weighted sum of ^{1}H and ^{15}N chemical shift changes was calculated with the equation $\Delta\delta_{wei} = \Delta\delta(^{1}HN) + 0.2\,\Delta\delta(^{15}N)$.

Cross-saturation Experiments—In the cross-saturation experiments (19, 20) we prepared a sample containing LolA or mLolB labeled with ^{2}H and ^{15}N and the unlabeled binding partner. The molar ratio of the unlabeled protein to the labeled protein was set to 4:1. Saturation transfer from the unlabeled protein to the labeled protein was made using the WURST decoupling scheme with the saturation frequency set at 0.833 ppm. The saturation time was 2.0 s, and relaxation delay was 2.0 s. All spectra were processed using nmrPipe (21). Data analysis was facilitated by the Sparky software (T. D. Goddard and D. G. Kneller, Sparky 3, University of California, San Francisco).

Spin-labeling Experiments—For site-directed spin labeling, five single Cys substituted mutants of LolA, *i.e.* V24C, V32C, I58C, L59C, and Q145C, were prepared. The proteins were modified with the spin-label reagent MTSL ((1-oxyl-2,2,5,5-tetramethyl-Δ^3-pyrroline-3-methyl)methanethiosulfonate) (Toronto Research Chemicals), which attaches the nitroxide spin label via a disulfide bond to the single cysteine (22). The spin label reagent MTSL in acetonitrile was added to the solution of each LolA mutant at a molar ratio of 7–8:1 (MTSL:LolA) and incubated at 25 °C for 20–24 h. After the reaction, the buffer was changed to buffer B, and the excess MTSL was removed. The molar ratio of each spin-labeled LolA to ^{15}N-

[2] The abbreviations used are: PRE, paramagnetic relaxation enhancement; MTSL, (1-oxyl-2,2,5,5-tetramethyl-Δ^3-pyrroline-3-methyl)methanethiosulfonate; TROSY, transverse relaxation-optimized spectroscopy.

labeled mLolB was set to 3:1, where no more chemical shift changes of ^{15}N-labeled mLolB occurred. ^{1}H,^{15}N TROSY spectra of ^{15}N-labeled mLolB with each spin-labeled LolA were recorded before and after the MTSL was reduced by an incubation with ascorbate (Wako) at room temperature for 2 h.

RESULTS

Inhibitory Effect of Decanoate on Lipoprotein Transportation—The analyses of lipoprotein interactions with LolA and LolB are important to elucidate the molecular mechanism of lipoprotein localization. However, no structural information about the interaction is currently available because of the low aqueous solubility of the lipoproteins due to their acyl chains. In the present study we used a saturated fatty acid as an analogue of the acyl chains of lipoproteins. In the major lipoproteins a saturated hydrocarbon with 16 carbon atoms is most frequently adopted as the acyl chains (23, 24). However, the aqueous solubility of the saturated fatty acid with 16 carbon atoms, palmitic acid, was less than 0.5 mM at room temperature, which was too low to perform NMR analyses. On the other hand, decanoate, a saturated fatty acid with 10 carbon atoms, possesses the sufficient solubility of more than 200 mM and is suitable for the NMR experiments.

To assess the validity of the use of decanoate as the analogue of an acyl chain of the lipoprotein, we examined the inhibitory effect of decanoate on the lipoprotein (L10P) transfer activity of mLolB (Fig. 1). The amount of L10P incorporated into the outer membrane decreased depending on the concentration of decanoate preincubated with mLolB. These results suggested that the lipoprotein transfer reactions from LolA to mLolB and/or mLolB to outer membranes are sensitive to decanoate.

Decanoate Binding Sites on LolA and mLolB—To determine the decanoate binding sites on LolA and mLolB, chemical shift perturbation experiments were performed (Fig. 2) (supplemental Fig. S2). Here we calculated the weighted chemical shift changes ($\Delta\delta_{wei}$) using the equation (25, 26) $\Delta\delta_{wei} = \Delta\delta(^{1}HN) + 0.2\,\Delta\delta(^{15}N)$. Upon the addition of 5 mM decanoate, 11 residues (supplemental Table S1) of LolA showed $\Delta\delta_{wei}$ of >0.1 ppm. Among the affected residues, Gly-86 is located on the loop preceding α-helix 2. Phe-90 and Met-91 are located on α-helix 2, embedded in the hydrophobic cavity. The other affected residues are located on β-strands 1–2, 9, and 11 (Fig. 2*A*). Among the 11 affected residues, 6 hydrophobic residues are located in the core of the molecule, and their side chains are directed toward the concave side of the β-barrel. Although the other affected residues, Gln-33, Gly-86, Thr-128, Lys-155, and Ser-156, direct their side chains toward the outside of the protein surface, the amide groups of Gly-86, Thr-128, Lys-155, and Ser-156 are in close proximity to the affected hydrophobic residues. The observation that the residues with substantial chemical shift changes were mainly located inside the concave surface indicates that LolA accommodates decanoate on the concave side.

Upon the addition of decanoate, 12 residues (supplemental Table S1) of LolB showed $\Delta\delta_{wei}$ of >0.4 ppm. These residues are located on α-helices 2–3, β-strands 1–2, 9, and 11 (Fig. 2*B*). Among the 12 affected residues, Ale-38 and Thr-55 direct their side chains to the convex side of the β-barrel, whereas the other residues direct their side chains toward the concave side of the β-barrel. Interestingly, the side chains of Thr-105, Met-107, Leu-114, and Ile-118 are located in close proximity to the binding site of PEGMME2000 found in the crystal structure, suggesting that decanoate and PEGMME2000 bind to LolB in a similar manner.

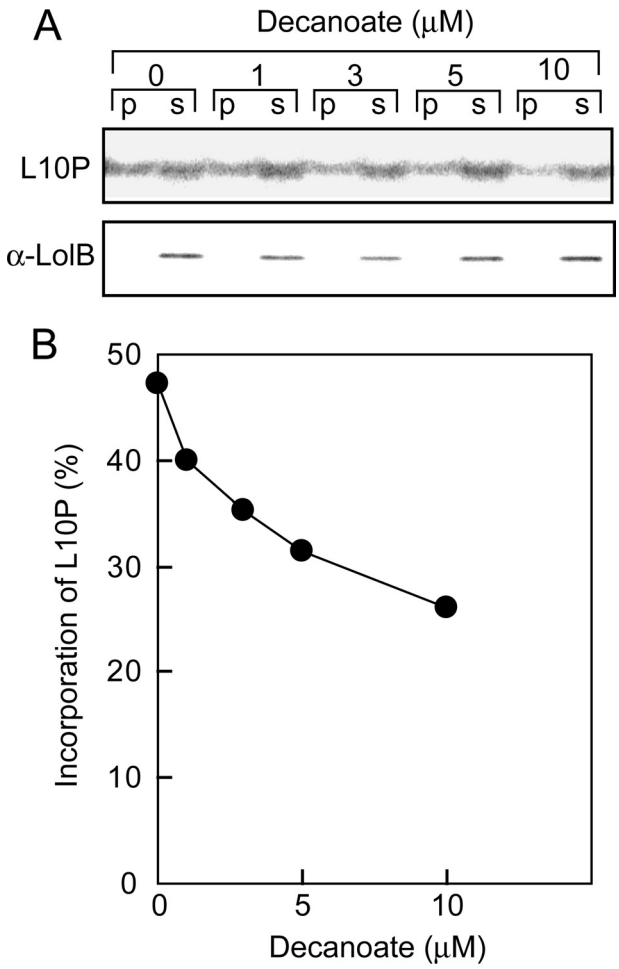

FIGURE 1. **Decanoate inhibits the LolA/LolB-dependent outer membrane incorporation of lipoproteins.** A spheroplast supernatant containing the LolA·[^{35}S]L10P complex was mixed with LolB-depleted outer membranes. To 90 μl of this mixture, 10 μl of a mLolB solution pretreated with the indicated concentrations of decanoate was added and incubated at 30 °C for 1 h as described under "Experimental Procedures." *A*, reaction mixtures were fractionated into pellet (*p*) and supernatant (*s*) followed by SDS-PAGE and fluorography (*L10P*) or immunoblotting (*LolB*). *B*, the amounts of L10P incorporated into outer membranes were densitometrically quantified and are expressed as percentages, considering the total amount of L10P as 100%.

Binding Affinity of LolA to mLolB—Using isothermal titration calorimetry analyses, we determined the dissociation constant K_d of LolA for mLolB. The analysis revealed a K_d value of 30.7×10^{-6} M and a stoichiometry of 1.1 mol mLolB/mol of LolA. These results indicate that LolA and mLolB can specifically interact with each other even in the absence of a lipoprotein.

Resonance Assignments for the LolA·mLolB Complex—By using LolA uniformly labeled with ^{2}H, ^{13}C, and ^{15}N ([^{13}C/^{2}H/^{15}N]LolA) and mLolB labeled with ^{2}H and ^{15}N ([^{2}H/^{15}N]mLolB), we recorded ^{1}H,^{15}N TROSY spectra. The superimposed ^{1}H,^{15}N TROSY spectra of [^{13}C/^{2}H/^{15}N]LolA

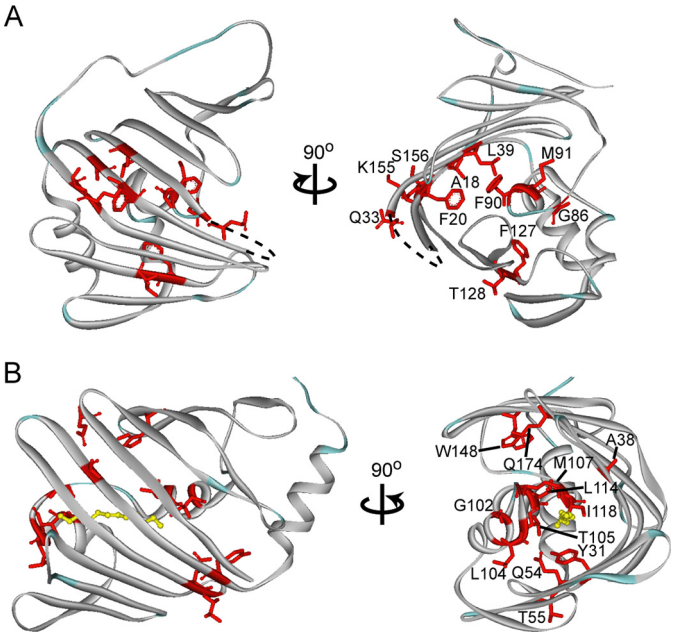

FIGURE 2. **Mapping of the LolA and mLolB residues affected by the titration of decanoate.** LolA residues with $\Delta\delta_{wei} > 0.1$ ppm (*A*) and mLolB residues with $\Delta\delta_{wei} > 0.4$ ppm (*B*) upon the addition of 5 mM decanoate are colored *red* and labeled. The PEGMME2000 molecule is colored *yellow*.

(Fig. 3*A*) and [^{2}H/^{15}N]mLolB (Fig. 3*B*) with various amounts of the binding partner are shown. We previously established the backbone resonance assignments of [^{13}C/^{2}H/^{5}N]LolA and [^{2}H/^{15}N]mLolB in their free states (13, 14). The backbone resonance assignments of [^{13}C/^{2}H/^{5}N]LolA and [^{2}H/^{15}N]mLolB complexed with each binding partner were determined by following the chemical shift changes upon the titration of each binding partner. Triple-resonance experiments were also performed to confirm the assignments of the complexed forms. Of 175 non-proline residues in LolA and mLolB, 82 and 84% of the resonances originating from the backbone amide groups could be assigned in their bound states, respectively, although the other resonance assignments could not be established, mainly because of line-broadening upon the addition of the binding partner.

Upon the addition of a 3-fold molar ratio of mLolB, 34 residues of LolA exhibited $\Delta\delta_{wei}$ of >0.3 ppm, and 20 residues of LolA showed $\Delta\delta_{wei}$ of 0.2–0.3 ppm (supplemental Table S2). In addition, the cross-peaks originating from 16 residues of LolA disappeared upon the addition of mLolB.

Upon the addition of a 3-fold molar ratio of LolA, 12 residues of mLolB exhibited $\Delta\delta_{wei}$ of >0.3 ppm, and 9 residues of mLolB showed $\Delta\delta_{wei}$ of 0.2–0.3 ppm (supplemental Table S2). In addition, the cross-peaks originating from nine residues of mLolB disappeared upon the addition of LolA.

Interfacial Residues of the LolA·mLolB Complex—To identify the residues located on the interface between LolA and mLolB in the complex, we used cross-saturation methods. Either LolA or mLolB labeled with ^{2}H, ^{15}N, and/or ^{13}C was bound to its unlabeled binding partner. LolA/mLolB molecule-selective saturation was achieved by applying the radio frequency irradiation centered at 0.833 ppm, which corresponds to the CH_2/CH_3 protons within the non-labeled protein.

Residue-selective signal intensity reductions were observed with an irradiation length of 2.0 s. Among the 131 analyzed signals originating from the main chain amide groups of LolA, three signals from Val-32, Gln-75, and Gln-145 exhibited intensity reduction ratios of >0.5, and signals from 25 residues showed intensity reduction ratios from 0.3 to 0.5 (Fig. 4*A*) (residue lists in supplemental Table S3). The residues affected by the saturation are indicated on the crystal structure of LolA (Fig. 4*B*). Most of the affected residues were located along the edge of the β-barrel. Specifically, the N-terminal ends of β-strands 2, 6, 9, and 11, the C-terminal ends of β-strands 1 and 10, the middle regions of β-strands 3 and 5, and all of β-strand 4 are involved in the LolB recognition. In addition to the affected β-barrel residues, 2 residues on α-helix 2, Leu-92 and Ala-94, exhibited remarkable signal intensity reductions, indicating that α-helix 2 is part of the mLolB binding surface. Among the affected residues, five acidic residues, Glu-34, Glu-56, Asp-146, Asp-147, and Asp-178, and one basic residue, Arg-149, are located along the edge of the β-barrel structure.

Among the 123 analyzed signals originating from the main chain amide groups of mLolB, signals from 8 residues exhibited intensity reduction ratios of >0.5, and signals from 14 residues showed intensity reduction ratios from 0.3 to 0.5 (Fig. 5*A*) (residue lists are shown in supplemental Table S3). The affected residues are predominantly located on β-strands 1 and 2 and the loop connecting β-strands 5 and 6 (Fig. 5*B*). These residues are clustered in a limited area on the convex surface of the β-barrel of mLolB. The interfacial surface of mLolB includes six basic residues, whereas no acidic residue is present. Among the six basic residues, Arg-34, Lys-45, Arg-49, Arg-91, and Lys-177 are located on the β-strands. Lys-88 is located in the loop connecting β-strands 5 and 6. In contrast to LolA, the α-helices of mLolB in the complex are not affected, which indicates that the convex side of mLolB is involved in the interaction.

Relative Orientations of LolA and mLolB in the Complex—To determine the relative orientations of LolA and mLolB, we introduced site-directed spin-labeling and performed PRE experiments. This technique provides distance information from the spin center up to 20–25 Å (27). Spin labels were introduced at each of positions 24, 32, 58, 59, and 145 of LolA (Fig. 6*A*). The residues at these positions were identified as the interfacial residues by the cross-saturation method. The residues at positions 24, 32, and 145 are on the edge of the β-barrel. On the other hand, the residues at positions 58 and 59 are in the middle of the β-barrel. The side chain at position 58 is directed toward the convex side of the β-barrel, whereas the side chain at position 59 points toward the concave side of the β-barrel.

We recorded the ^{1}H,^{15}N TROSY spectra of ^{15}N-labeled mLolB complexed with LolA spin-labeled with MTSL in the presence and absence of a reducing agent, ascorbic acid, which reduces the spin-label agent covalently attached to each of the five positions of LolA. The chemical shifts of the amide resonances originating from mLolB complexed with each spin-labeled LolA in the reduced states were almost identical to those observed for mLolB complexed with the

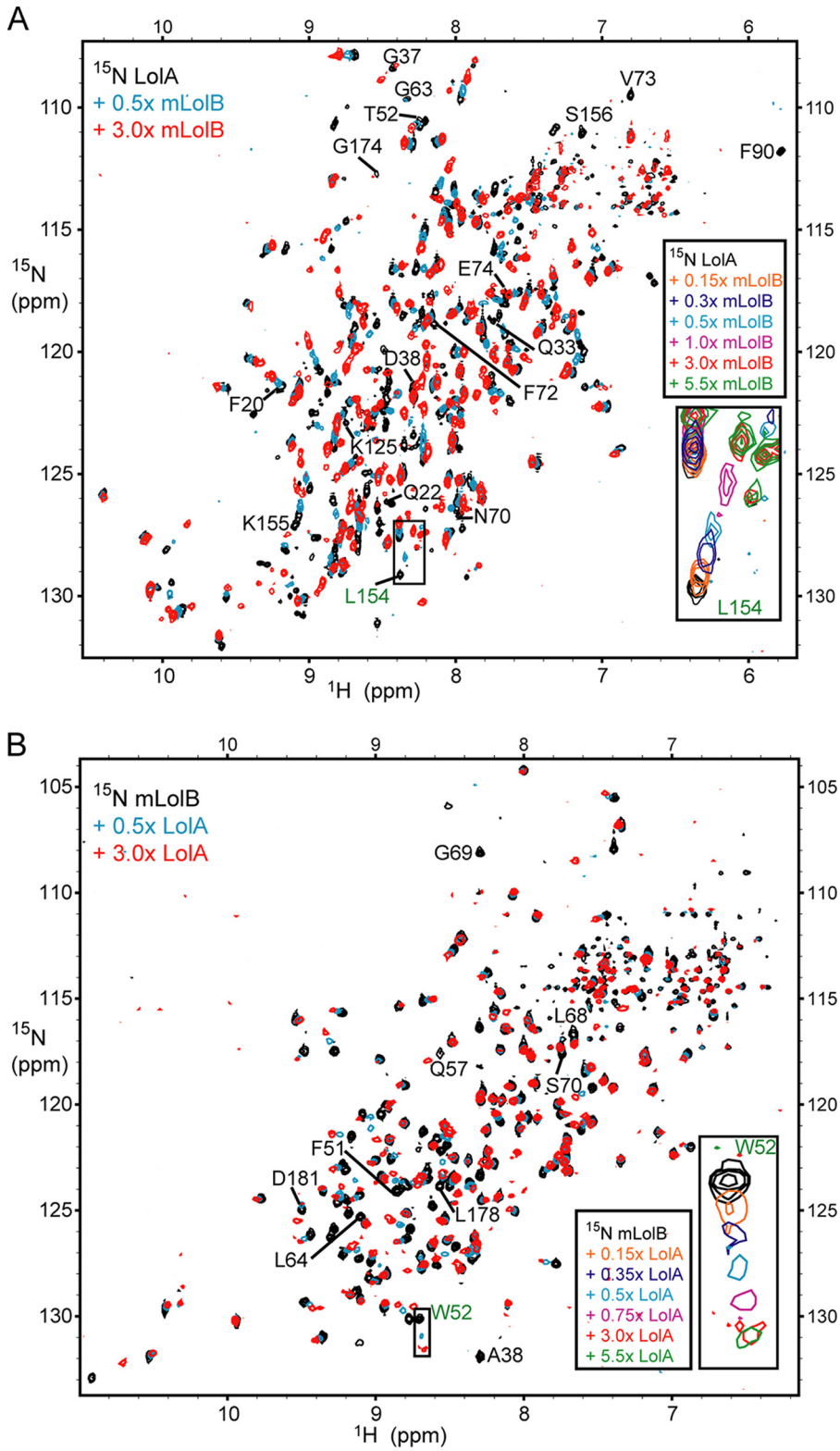

FIGURE 3. **Overlaid ^{1}H,^{15}N TROSY spectra of labeled LolA binding to unlabeled mLolB and labeled mLolB binding to unlabeled LolA.** Overlaid ^{1}H,^{15}N TROSY spectra of labeled LolA (*A*) and labeled mLolB (*B*) upon the addition of a 0 (*black*)-, 0.5 (*blue*)-, or 3-fold (*red*) molar ratio of the unlabeled binding partner, mLolB and LolA. Signals that disappeared upon the addition of the binding partner at binding saturation ratios (over a 3-fold molar ratio) are labeled with a *black one-letter code* for amino acids and a *residue number* (16 residues for LolA and 9 residues for mLolB). *Insets*, portions of the spectra at a series of concentrations of the unlabeled binding partner showing the signals of Leu-154 from LolA and Trp-52 from mLolB in *panels A* and *B*, respectively. The cross-peaks from the two residues clearly shifted dependent on the addition of the binding partner.

wild type LolA, suggesting that the cysteine mutations and the MTSL labeling for LolA exerted minimal influence on the conformations of LolA and mLolB and the binding mode between LolA and mLolB.

We compared the signal intensities of the spectra with and without ascorbic acid. The mLolB residues that showed marked signal intensity reductions are mapped on the crystal structure (Figs. 6, *B–F*) (complete lists of affected residues are shown in supplemental Table S4). Upon complex formation with LolA spin-labeled at position 24, the backbone amide signals originating from 11 residues were broadened to undetectable levels. The signal intensities of six residues were remarkably reduced (intensity ratio <0.3) (Fig. 6*B*). Upon complex formation with LolA spin-labeled at position 32, the signals originating from 18 residues disappeared. The signals from seven residues showed reduced intensities (intensity ratio <0.3) (Fig. 6*C*). Upon complex formation with LolA spin-labeled at position 59, the signals originating from eight residues were broadened to undetectable levels. The signal intensity of one residue, Tyr-39 was reduced (intensity ratio <0.3) (Fig. 6*E*). Upon complex formation with LolA spin-labeled at position 145, the signals originating from 10 residues were broadened to undetectable levels. The signal intensities of seven residues were reduced (intensity ratio <0.3) (Fig. 6*F*). In contrast, upon complex formation with LolA spin-labeled at position 58, only one residue on mLolB, Tyr-47, displayed a weak signal intensity reduction (intensity ratio <0.3) (Fig. 6*D*).

These selective signal intensity reductions suggest the spatial proximity of the affected mLolB residues to each spin-labeled position of LolA. The spin center at position 59, in the middle region of β-strand 4 of LolA, markedly affected the edge of the β-barrel of mLolB (Fig. 6*E*). On the other hand, the spin center located on the convex side at position 58 had only a minimal effect on mLolB

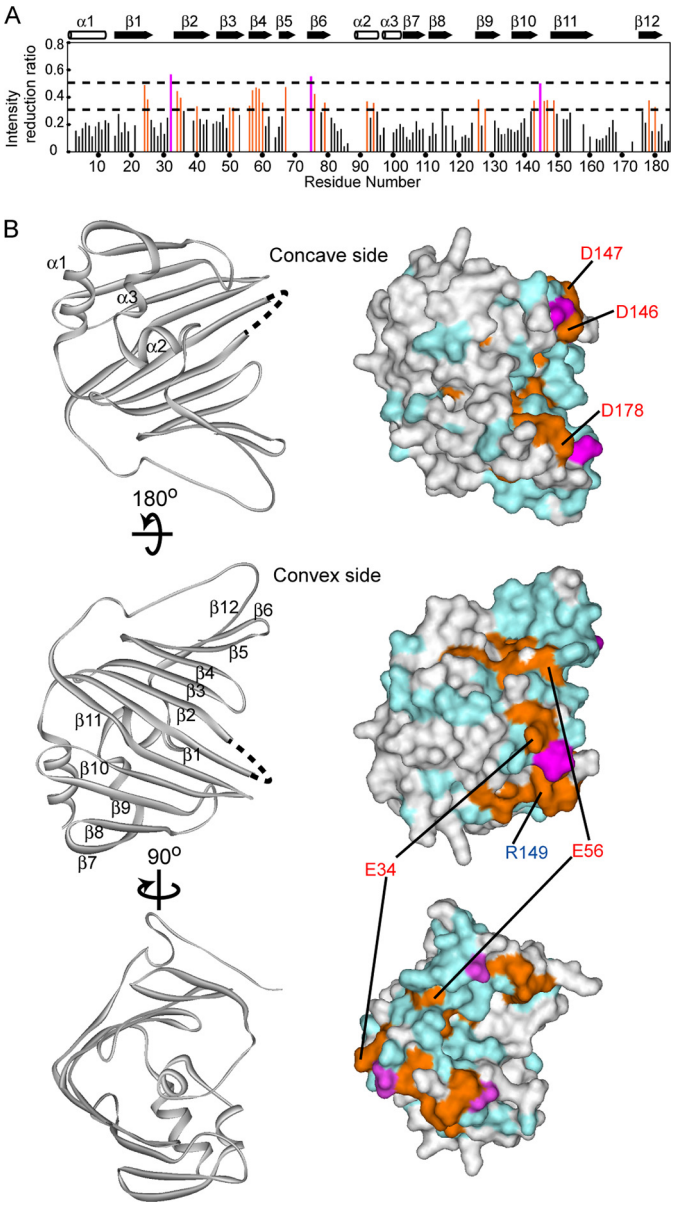

FIGURE 4. **Intensity reductions in the cross-saturation experiments and mapping of the interfacial residues on the crystal structure of LolA.** *A*, intensity reduction ratios of LolA residues in the cross-saturation experiments are displayed as *bars* (>0.5 colored pink; 0.3–0.5 colored orange). *B*, affected residues are mapped on the crystal structures (surface representations are in the *right panel*). The same coloring system is used as *panel A*. The affected acidic and basic residues are indicated with a *one-letter code* for amino acids and a *residue number*. Proline residues and residues unassigned in a complex state are colored *cyan*. The other residues that are assigned but unaffected are *white*.

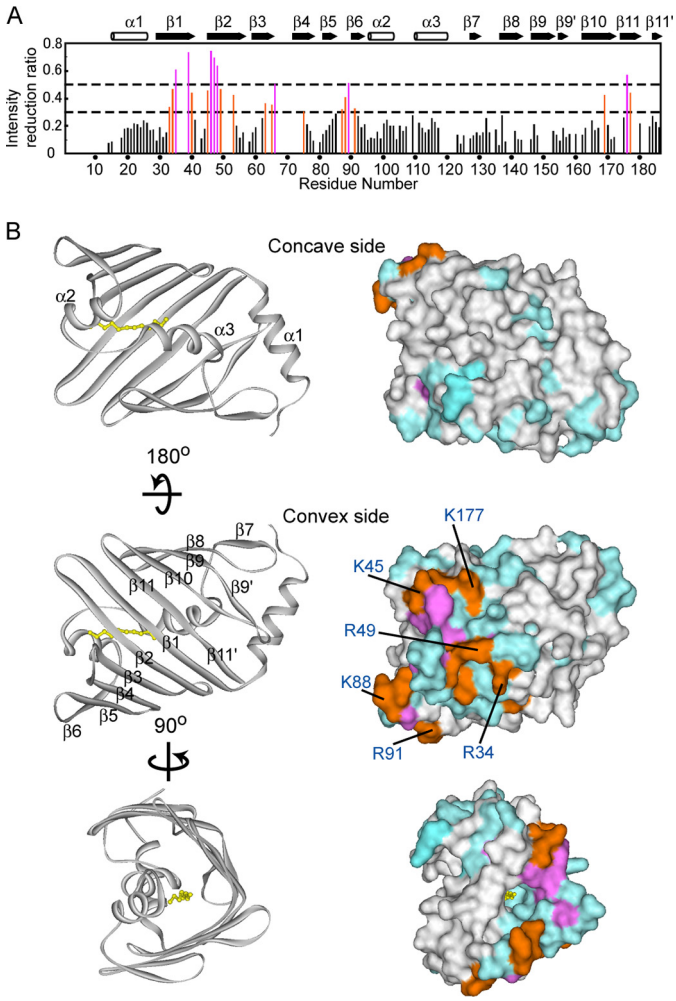

FIGURE 5. **Intensity reductions in the cross-saturation experiments and mapping of the interfacial residues on the crystal structure of mLolB.** *A*, intensity reduction ratios of mLolB residues in the cross-saturation experiments are displayed as *bars* (>0.5 colored *pink*; 0.3–0.5 colored *orange*). *B*, affected residues are mapped on the crystal structures (surface representations in the *right panel*). The same coloring system is used as *panel A*. The affected acidic and basic residues are indicated with a *one-letter code* for amino acids and a *residue number*. Proline residues and residues unassigned in a complex state are colored *cyan*. The other residues that are assigned but unaffected are *white*. The PEGMME2000 molecule is colored *yellow*.

(Fig. 6*D*). These results suggest that the concave side of the β-barrel of LolA interacts with mLolB. The spin centers at positions 24 and 32, located at the C-terminal end of β-strand 1, affected β-strands 1–4, 11, and 11′ of mLolB (Figs. 6, *B* and *C*). The spin center at position 145 at the C-terminal end of β-strand 10 of LolA affected β-strands 1–6 of mLolB (Fig. 6*F*). Therefore, the C-terminal end of β-strand 1 of LolA in the complex and the C-terminal end of β-strand 10 of LolA in the complex are located in close proximity to β-strand 1 and/or 2 of mLolB and to β-strand 3 and/or 4 of mLolB, respectively. None of the mLolB residues on α-helices 2 and 3, which reside on the concave face of the β-barrel, was affected by complex formation with the spin-labeled LolAs. Taken together, we concluded that the concave side of LolA interacts with the convex side of mLolB.

DISCUSSION

Understanding the molecular mechanism of the lipoprotein translocation process requires the structural basis for the interactions between the Lol proteins. Toward this goal, we have undertaken NMR studies, including the cross-saturation and PRE experiments, aimed at the structural characterizations of the interaction between LolA/LolB and an analogue of acyl chains of lipoproteins, decanoate, and the interaction between LolA and LolB.

Acyl Chain Accommodation within the Hydrophobic Cavity—Although it has been speculated that hydrophobic concave sides of LolA and LolB preferably accommodate the hydro-

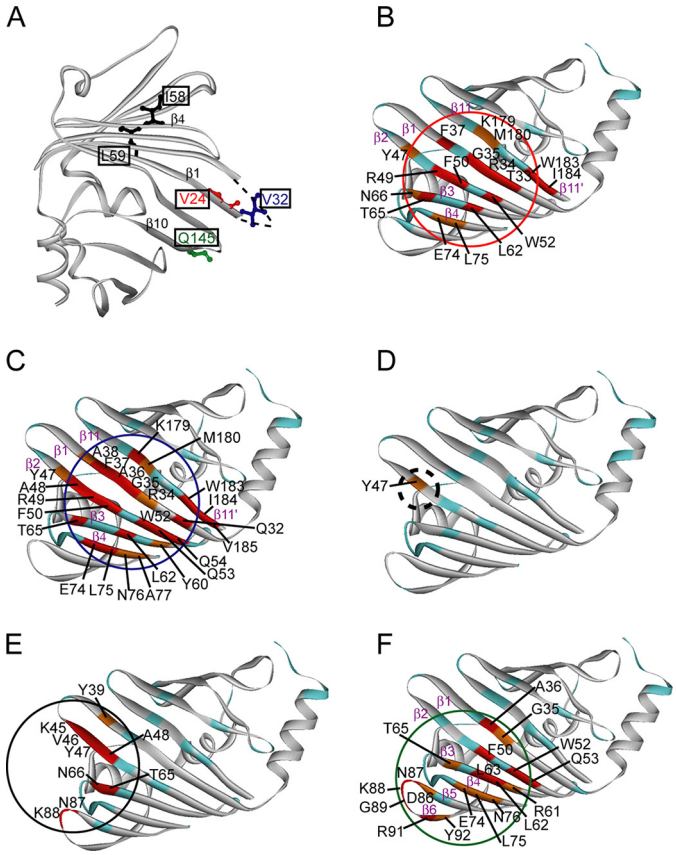

FIGURE 6. **Mapping of mLolB residues affected by spin-labeled variants of LolA.** *A*, the five residues of LolA that were each substituted with cysteine and spin-labeled with MTSL are indicated on the crystal structure. The residues of ^{15}N-labeled mLolB affected by the spin-labeled LolAs at position 24 (*B*), 32 (*C*), 58 (*D*), 59 (*E*), and 145 (*F*) are mapped on the crystal structures. Residues that showed no signals upon binding to each spin-labeled LolA are colored *red*. Residues that showed an intensity ratio <0.3 upon binding to each spin-labeled LolA are shown in *orange*. Proline residues and residues unassigned in a complex state are colored *cyan*. The other residues that are assigned but unaffected are *white*.

phobic acyl chain part of lipoproteins, there was no evidence to confirm this speculation. The chemical shift perturbations of LolA and mLolB upon the addition of decanoate, which was used as an analog of the acyl chain of lipoproteins, revealed that decanoate binds to the concave sides of the Lol proteins. Therefore, LolA and mLolB recognize the acyl chains of lipoproteins by using the hydrophobic area of the concave sides of the molecules and some conformational changes of LolA and mLolB, as the crystal structures of both proteins show insufficient space for accommodating three acyl chains.

Interaction between LolA and mLolB—The isothermal titration calorimetry experiments revealed that LolA and mLolB interact with each other even in the absence of a lipoprotein. It is likely that the LolA and mLolB molecules partially exist as the complexed form *in vivo*, although the biological significance of the complex remains unknown.

The cross-saturation experiments successfully identified the binding site of mLolB to LolA. mLolB recognized LolA using the convex side of the molecule. However, the cross-saturation data did not provide sufficient information about the binding mode of LolA, as the assignments of LolA in the bound form could not be established completely, mainly because of the broadening of the signals from the flexible nature of LolA (see below). Therefore, to determine the binding mode between LolA and mLolB in detail, we further observed the PREs from LolA to mLolB. The introduction of MTSL to the concave side of LolA caused remarkable PREs to the convex side of mLolB (Fig. 6*E*), suggesting that the concave side of LolA is responsible for mLolB binding.

Using the combination of the cross-saturation and PRE experiments, the interfacial residues in the LolA·mLolB complex and their relative orientations in the complex were identified. A central feature of the mLolB binding mode to LolA is that part of the concave side of the β-barrel of LolA is used for the binding of mLolB, and the remaining part is exposed to the solvent. The complete usage of the concave side of LolA for binding to mLolB is obstructed by α-helix 2, which serves as a plug. In contrast, the LolA binding site on mLolB is the convex side of the β-barrel, and no residue on three helices of mLolB was involved in the binding.

The electrostatic potential mapping of each protein supports our concave-convex interaction mode. Interestingly, the electrostatic potential map of LolA revealed that the concave side is predominantly composed of negatively charged residues (*circled* in supplemental Fig. S3). In contrast, the convex side of mLolB possesses positive charges. Therefore, it is most likely that the complementary electrostatic potential is responsible for the complex formation between LolA and mLolB.

The photo-cross-linking experiments suggested that some residues that were identified by the preset study exhibited the high efficiency of the cross-linking (28). Therefore, these observations also support the interaction mode.

Difference in the Affected Residues of LolA between the Cross-saturation and Chemical Shift Perturbation Experiments—It is impossible to make the LolA·mLolB complex model by using the currently available crystal structures because of steric hindrance. Therefore, either or both LolA/mLolB must undergo conformational changes upon complex formation.

To gain insights into the conformational changes, we compared the results of the cross-saturation experiments with those of the chemical shift perturbation experiments. The weighted sum of the chemical shift changes of the backbone amide protons and nitrogen atoms of LolA and mLolB caused by binding to the binding partner are summarized (Figs. 7*A* and 8*A*).

The residues that displayed the chemical shift perturbation upon complex formation are indicated on the crystal structures (Figs. 7*B* and 8*B*). The affected LolA residues are spread all over the β-barrel (Fig. 7*B*). In contrast, the residues of mLolB with the substantial chemical shift perturbations upon LolA binding were almost identical to the interfacial residues identified in the cross-saturation experiments (Figs. 5*B* and 8*B*).

Considering the fact that the chemical shift perturbations reflect secondary effects, which are the effects of the conformational changes caused by binding as well as the direct effects of the binding, we conclude that LolA undergoes a conformational change of its β-barrel to an open form upon

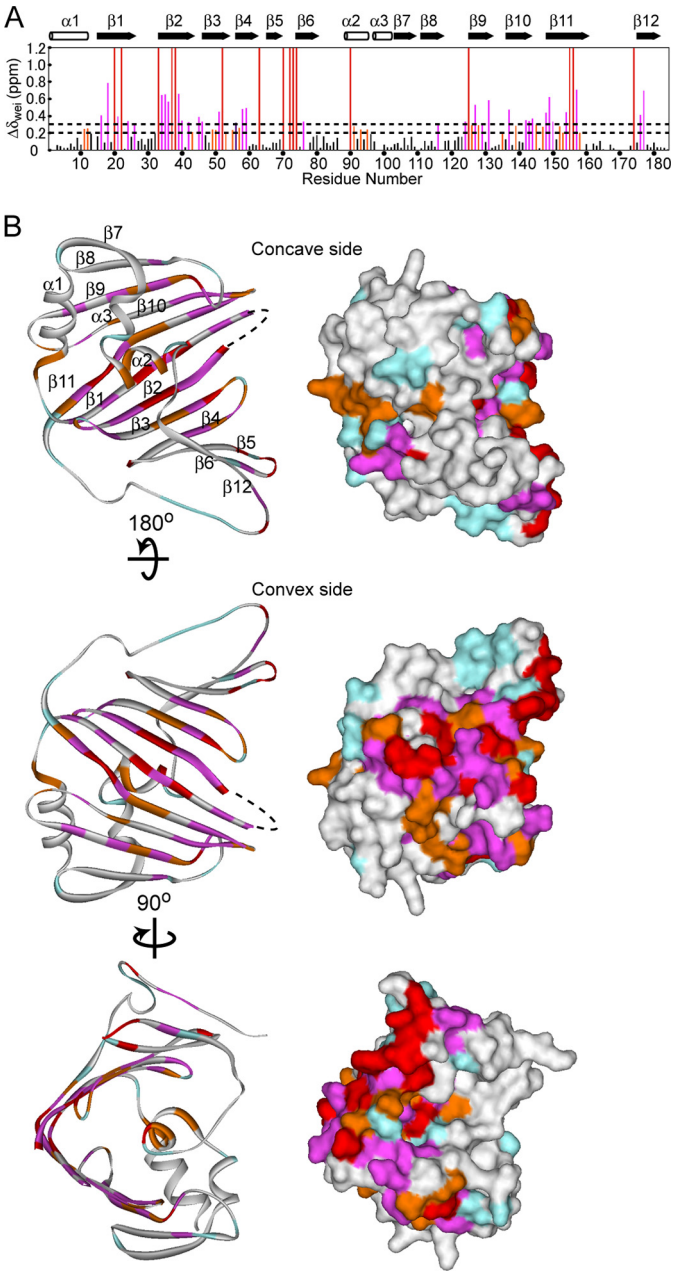

FIGURE 7. **Chemical shift changes of LolA amide groups upon the addition of mLolB and mapping of affected residues on the crystal structure.** *A*, the weighted sum of the chemical shift changes ($\Delta\delta_{wei}$) of the backbone amide resonances from LolA upon the addition of mLolB. *Orange* and *pink bars* indicate residues with $\Delta\delta_{wei}$ of 0.2–0.3 and $\Delta\delta_{wei}$ >0.3 ppm, respectively. *Red bars* indicate residues that disappeared upon complex formation. *B*, the affected residues in the chemical shift perturbation experiments are mapped on the crystal structures of LolA (*ribbon* representations in the *left panel*, surface representations in the *right panel*). The same coloring system is used as *panel A*. Proline residues and unassigned residues in a free state are colored *cyan*. The other residues that are assigned but unaffected are *white*.

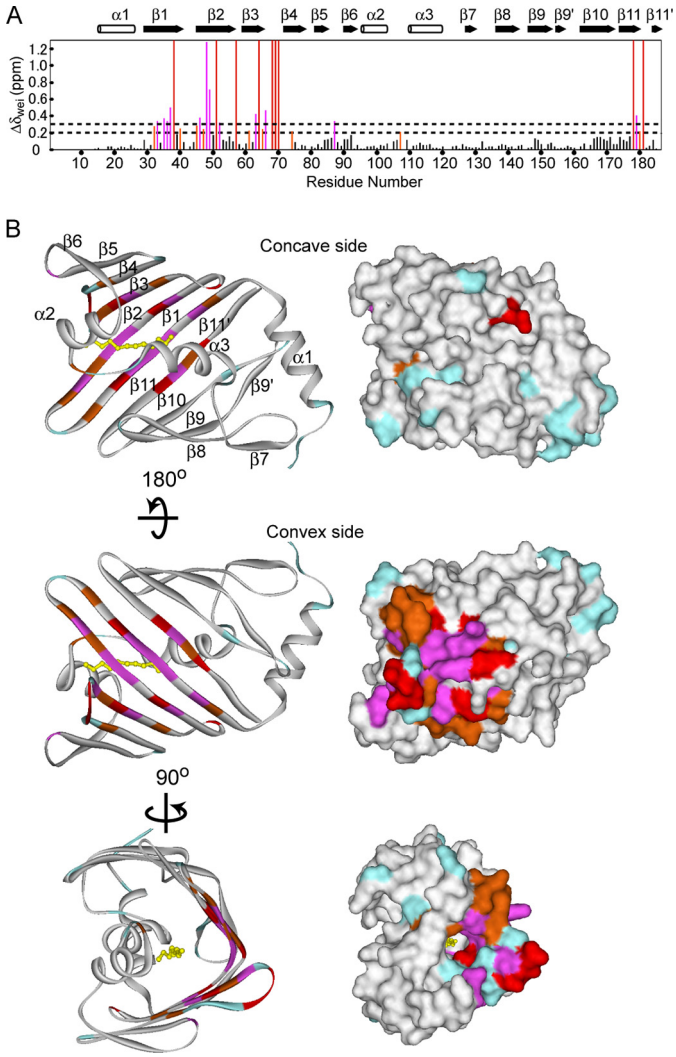

FIGURE 8. **Chemical shift changes of mLolB amide groups upon the addition of LolA and mapping of affected residues on the crystal structure.** *A*, the weighted sum of the chemical shift changes ($\Delta\delta_{wei}$) of the backbone amide resonances from mLolB upon the addition of LolA. *Orange* and *pink bars* indicate residues with $\Delta\delta_{wei}$ of 0.2–0.3 and $\Delta\delta_{wei}$ >0.3 ppm, respectively. *Red bars* indicate residues that disappeared upon complex formation. *B*, the affected residues in the chemical shift perturbation experiments are mapped on the crystal structures of mLolB (ribbon representations are shown in the *left panel*, and surface representations are shown in the *right panel*). The same coloring system is used as *panel A*. Proline residues and unassigned residues in a free state are colored *cyan*. The other residues that are assigned but unaffected are *white*.

mLolB binding as represented in Fig. 9, whereas the structure of mLolB does not. We also observed a substantial difference in the hydrogen/deuterium (H/D) exchange rates of the amide groups between LolA and mLolB in the free state (supplemental "Experimental Procedures" and Fig. S4). This observation suggests that LolA exhibits higher plasticity than mLolB, supporting the conformational changes of LolA upon complex formation. Furthermore, we measured $^{13}C^{\alpha}$ and $^{13}C^{\beta}$ chemical shifts of labeled LolA in the presence and absence of unlabeled mLolB. The small but substantial changes in the $^{13}C^{\alpha}$ and $^{13}C^{\beta}$ chemical shifts of LolA were observed upon binding of mLolB (supplemental Fig. S5), suggesting that some conformational changes occur. In the LolA·mLolB binding mode suggested by the present study, a contiguous hydrophobic surface, which is composed of part of the concave side of LolA and mLolB, is generated upon complex formation.

Lipoprotein Transfer from LolA to LolB—On the basis of the NMR analyses, we propose the following mechanism of lipoprotein transfer from LolA to LolB (Fig. 9). 1) LolA receives a lipoprotein from the Lol·CDE complex in the inner

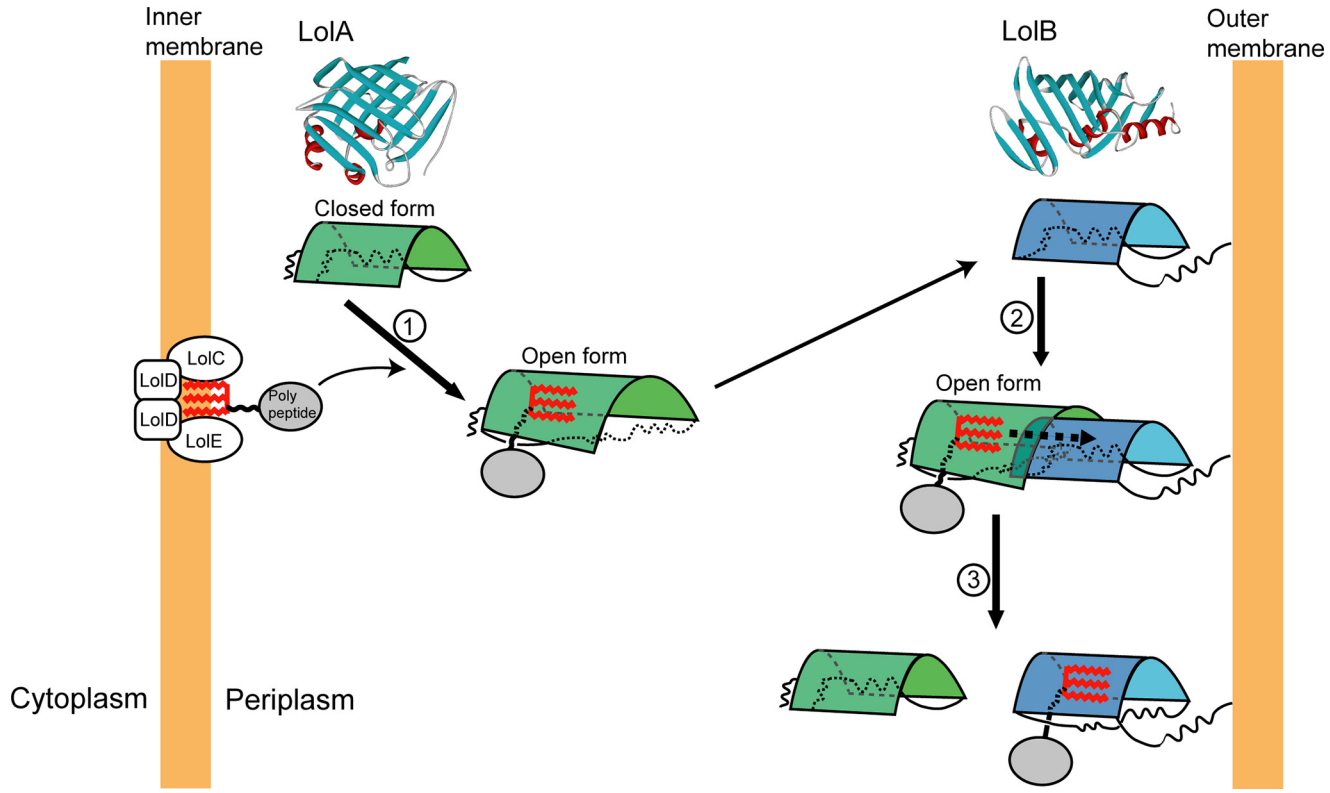

FIGURE 9. **Schematic illustration of the interaction between LolA and LolB and a lipoprotein transfer model.** The β-barrels of LolA and mLolB are graphically represented and are colored *green* and *blue*, respectively. The acyl chain moiety is colored *red*. In step 1 LolA receives a lipoprotein from Lol·CDE, which is anchored to the outer face of the inner membrane. LolA undergoes conformational changes and accommodates one to three of the lipoprotein acyl chains inside the hydrophobic cavity. In step 2, the lipoprotein-bound LolA interacts with LolB, which is anchored to the outer membrane. In the complex, LolA and LolB form a hydrophobic, tunnel-like structure. In step 3, the acyl chains accommodated within the cavity of LolA are transferred from LolA to LolB through the hydrophobic tunnel formed by the two proteins.

membrane. In the LolA-lipoprotein complex, LolA accommodates the acyl chains of the lipoprotein on its hydrophobic concave side and undergoes some conformational changes (29, 30). LolA then transports the lipoprotein from the inner to the outer membrane. 2) The LolA-lipoprotein complex interacts with LolB, which is anchored to the inner side of the outer membrane. In the LolA·LolB complex, the concave side of the β-barrel of LolA contacts with the convex side of the β-barrel of LolB. Accordingly, the hydrophobic insides of LolA and LolB are connected, and a hydrophobic tunnel-like structure is formed. 3) The acyl chains in LolA are smoothly transferred through the hydrophobic tunnel, from LolA to LolB.

The driving force of the lipoprotein transfer from LolA to LolB might simply be the higher affinity of a lipoprotein for LolB than for LolA. Good evidence for this can be found in the previous study (31). They revealed that an outer membrane-directed lipoprotein, Pal, forms a tighter complex with mLolB than with LolA. Therefore, the difference in the affinities between LolA and LolB is responsible for the lipoprotein transfer in the complex.

Although several fatty acid-protein interactions have been investigated based on the structural analysis (32), only limited structural information about protein-protein or protein-membrane interactions involving the fatty acid-binding proteins has been available. Our clarification of the interactions between the lipoprotein-binding proteins may provide new insights into these aspects of fatty acid-interacting proteins.

Acknowledgments—We thank Mr. Iwao Fujiwara, Dr. Yukio Tominaga, and Dr. Masuo Kurono for continuous support and helpful discussions.

REFERENCES

1. Tokuda, H., Matsuyama, S., and Tanaka-Masuda, K. (2007) in *The Periplasm* (Ehrmann, M., ed) pp. 67–79, American Society for Microbiology, Washington, D. C.
2. Fraser, C. M., Casjens, S., Huang, W. M., Sutton, G. G., Clayton, R., Lathigra, R., White, O., Ketchum, K. A., Dodson, R., Hickey, E. K., Gwinn, M., Dougherty, B., Tomb, J. F., Fleischmann, R. D., Richardson, D., Peterson, J., Kerlavage, A. R., Quackenbush, J., Salzberg, S., Hanson, M., van Vugt, R., Palmer, N., Adams, M. D., Gocayne, J., Weidman, J., Utterback, T., Watthey, L., McDonald, L., Artiach, P., Bowman, C., Garland, S., Fuji, C., Cotton, M. D., Horst, K., Roberts, K., Hatch, B., Smith, H. O., and Venter, J. C. (1997) *Nature* **390,** 580–586
3. Braun, V., and Wu, H. C. (1994) in *Bacterial Cell Wall* (Ghuysen, J.-M., and Hakenbeck, R., eds) pp. 319–341, Elsevier Science Publishers B. V., Amsterdam
4. Pugsley, A. P. (1993) *Microbiol. Rev.* **57,** 50–108
5. Yakushi, T., Yokota, N., Matsuyama, S., and Tokuda, H. (1998) *J. Biol. Chem.* **273,** 32576–32581
6. Yakushi, T., Masuda, K., Narita, S., Matsuyama, S., and Tokuda, H. (2000) *Nat. Cell Biol.* **2,** 212–218
7. Narita, S., Tanaka, K., Matsuyama, S., and Tokuda, H. (2002) *J. Bacteriol.* **184,** 1417–1422

8. Matsuyama, S., Yokota, N., and Tokuda, H. (1997) *EMBO J.* **16,** 6947–6955
9. Yokota, N., Kuroda, T., Matsuyama, S., and Tokuda, H. (1999) *J. Biol. Chem.* **274,** 30995–30999
10. Tanaka, K., Matsuyama, S. I., and Tokuda, H. (2001) *J. Bacteriol.* **183,** 6538–6542
11. Takeda, K., Miyatake, H., Yokota, N., Matsuyama, S., Tokuda, H., and Miki, K. (2003) *EMBO J.* **22,** 3199–3209
12. Narita, S., Kanamaru, K., Matsuyama, S., and Tokuda, H. (2003) *Mol. Microbiol.* **49,** 167–177
13. Nakada, S., Takahashi, H., Sakakura, M., Kurono, M., and Shimada, I. (2007) *Biomol. NMR Assign.* **1,** 125–127
14. Nakada, S., Sakakura, M., Takahashi, H., Tokuda, H., and Shimada, I. (2007) *Biomol. NMR. Assign.* **1,** 121–123
15. Matsuyama, S., Tajima, T., and Tokuda, H. (1995) *EMBO J.* **14,** 3365–3372
16. Yakushi, T., Tajima, T., Matsuyama, S., and Tokuda, H. (1997) *J. Bacteriol.* **179,** 2857–2862
17. Terada, M., Kuroda, T., Matsuyama, S. I., and Tokuda, H. (2001) *J. Biol. Chem.* **276,** 47690–47694
18. Wada, R., Matsuyama, S., and Tokuda, H. (2004) *Biochem. Biophys. Res. Commun.* **323,** 1069–1074
19. Takahashi, H., Nakanishi, T., Kami, K., Arata, Y., and Shimada, I. (2000) *Nat. Struct. Biol.* **7,** 220–223
20. Nakanishi, T., Miyazawa, M., Sakakura, M., Terasawa, H., Takahashi, H., and Shimada, I. (2002) *J. Mol. Biol.* **318,** 245–249
21. Delaglio, F., Grzesiek, S., Vuister, G. W., Zhu, G., Pfeifer, J., and Bax, A. (1995) *J. Biomol. NMR* **6,** 277–293
22. Berliner, L. J., Grunwald, J., Hankovszky, H. O., and Hideg, K. (1982) *Anal. Biochem.* **119,** 450–455
23. Hantke, K., and Braun, V. (1973) *Eur. J. Biochem.* **34,** 284–296
24. Sankaran, K., and Wu, H. C. (1994) *J. Biol. Chem.* **269,** 19701–19706
25. Hajduk, P. J., Dinges, J., Miknis, G. F., Merlock, M., Middleton, T., Kempf, D. J., Egan, D. A., Walter, K. A., Robins, T. S., Shuker, S. B., Holzman, T. F., and Fesik, S. W. (1997) *J. Med. Chem.* **40,** 3144–3150
26. Meyer, B., and Peters, T. (2003) *Angew. Chem. Int. Ed. Engl.* **42,** 864–890
27. Gillespie, J. R., and Shortle, D. (1997) *J. Mol. Biol.* **268,** 158–169
28. Okuda, S., and Tokuda, H. (2009) *Proc. Natl. Acad. Sci. U.S.A.* **106,** 5877–5882
29. Watanabe, S., Oguchi, Y., Takeda, K., Miki, K., and Tokuda, H. (2008) *J. Biol. Chem.* **283,** 25421–25427
30. Oguchi, Y., Takeda, K., Watanabe, S., Yokota, N., Miki, K., and Tokuda, H. (2008) *J. Biol. Chem.* **283,** 25414–25420
31. Taniguchi, N., Matsuyama, S., and Tokuda, H. (2005) *J. Biol. Chem.* **280,** 34481–34488
32. Hamilton, J. A. (2004) *Prog. Lipid. Res.* **43,** 177–199